Applications of Adaptive Spacetime Meshing in the Asynchronous Spacetime Discontinuous Galerkin Method

Reza Abedi[1,*], **Robert B Haber**[2]

[1]Department of Mechanical, Aerospace & Biomedical Eng., University of Tennessee, Knoxville, USA
[2]Department of Mechanical Science & Engineering, University of Illinois, Urbana, USA

[*]Email: rabedi@utk.edu

Abstract

Asynchronous Spacetime Discontinuous Galerkin (aSDG) methods use robust adaptive meshing to construct unstructured grids on spacetime analysis domains with no global time-step constraints. While traditional adaptive remeshing is performed only once per N time steps, aSDG solvers perform many thousands of adaptive operations per layer of spacetime elements to capture fast-moving wavefronts and track rapidly-evolving interfaces. We present applications in dynamic fracture and electromagnetics to demonstrate these capabilities.

Keywords: adaptive meshing, spacetime, discontinuous Galerkin, front capturing, interface tracking, dynamic fracture, electromagnetics

1 Introduction

The *Tent Pitcher* algorithm [1] is the point of departure for aSDG adaptive meshing. Tent Pitcher advances a space-like *front mesh* with non-uniform time coordinates by incrementing the time coordinate of one vertex at a time. The increment of time advancement is limited by a *causality constraint* that ensures that the front remains space-like. Tessellations of the spacetime volume between fronts define *patches* of spacetime elements on which local aSDG solutions are computed. If the solution is successful, the old front is discarded and the process repeats on updated fronts until the spacetime analysis domain is covered.

Adaptive refinement is triggered whenever a patch solution fails adaptive error criteria. In that case, the adaptive meshing procedure discards the failed patch and the updated front, locally refines the old front mesh, and resumes the Tent Pitcher procedure. The result is new patches that are simultaneously refined in space and time. In addition to front refinement, adaptive vertex-deletion, edge-flip, and vertex-moving operations are available.

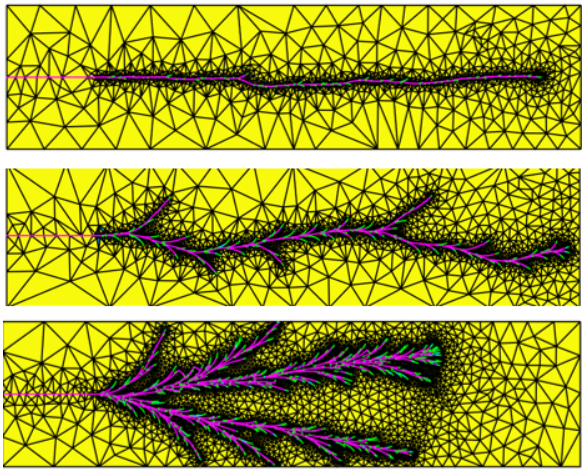

Figure 1: Dynamic tensile fracture under increasing load amplitudes.

2 Dynamic fracture: tracking interfaces

Simulation of dynamic fracture poses significant challenges: capturing fast-moving crack-tip fields and wavefronts as well as fracture nucleation, extension, and coalescence — all while ensuring that the physics model alone determines the crack patterns. We combined aSDG adaptive meshing capabilities with a stochastic fracture nucleation model to meet these challenges.

Figure 1 shows crack patterns due to dynamic fracture in identical pre-cracked strips subject to increasing mode-I load amplitudes. For the lowest loading (top), crack extension in nearly a straight line is sufficient to absorb the applied energy. As the loading increases (middle, bottom), so do crack-path undulation, micro-crack formation, and crack branching. The emergence of these mechanisms are also observed experimentally; they serve as means to dissipate excess input power.

Figure 2 compares predicted fracture patterns for homogeneous and inhomogeneous fracture strength. Crack nucleation is pervasive for homogeneous fracture strength, as in Fig. 2(a). A more realistic sparse nucleation pattern emerges for inhomogeneous fracture strength in Figs. 2(b) and 2(c) where only the weakest flaws trigger

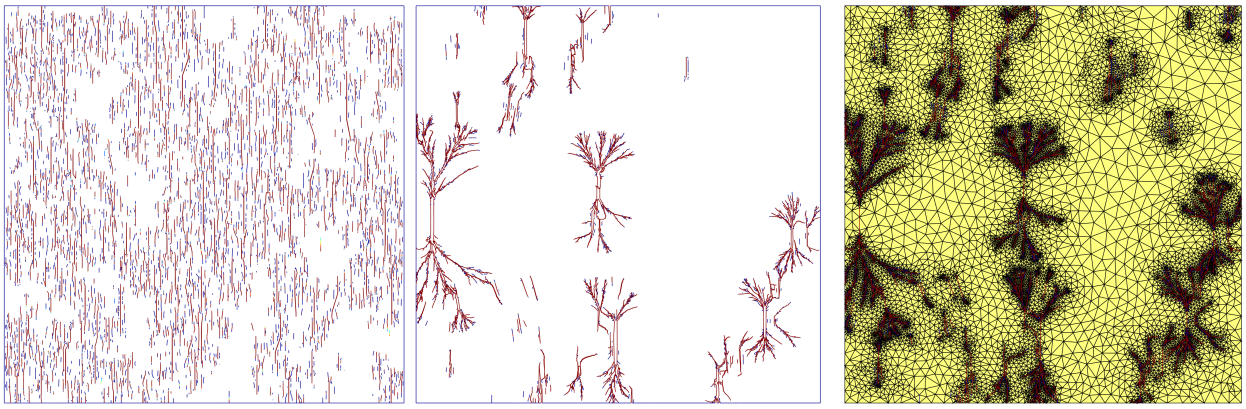

(a) Homogeneous strength. (b) Inhomogeneous strength (c) Inhomogeneous strength (mesh)

Figure 2: Effects of inhomogeneous fracture strength on fragmentation patterns

failure.

3 Electromagnetics: capturing wavefronts

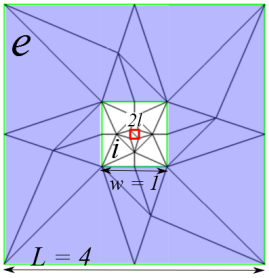

The two-dimensional *Transverse Magnetic* electromagnetic problem depicted at the right involves an inner square region filled with a low-electric-permittivity material (white) and an outer region containing a second material (purple) with 10 times higher electric permittivity. A short-duration excitation within the red square at the center of the domain generates a sharp wavefront that propagates to the bi-material interface where it is reflected and transmitted into the outer region.

We compare non-adaptive and adaptive aSDG simulations to demonstrate the flexibility and efficiency of asynchronous spacetime meshing. The non-adaptive front is, at all times, an unstructured mesh of 83071 triangles. The initial front mesh for the adaptive simulation with just 46 triangles is shown in the figure. We depend on adaptive spacetime meshing to generate sufficient refinement to capture the initial pulse as well as evolving patterns of sharp wavefronts over the course of the simulation, as depicted by the sequence in Fig. 3. The adaptive run generates 2.77 million patches over the course of the simulation with a minimum element diameter of 9.77×10^{-4}. This compares favorably with the non-adaptive run's minimum element diameter, 0.0134, as well as 5.6 times more patches, 7.5 times higher computation time, and about double the energy error of the adaptive simulation.

4 Conclusions

Adaptive aSDG methods support front capturing and interface tracking in some of the most challenging dynamic simulations. We will present additional examples that showcase emerging parallel–adaptive and 3d×time aSDG technologies.

References

[1] R. Abedi, S.-H. Cheng, J. Erickson, Y. Fan, M. Garland, D. Guoy, R. Haber, J. Sullivan, S. Thite and Y. Zhou. Spacetime meshing with adaptive refinement and coarsening, in *20th Ann Symp Comp Geometry, New York, USA, June 8–11, 2004*, pp. 300–309.

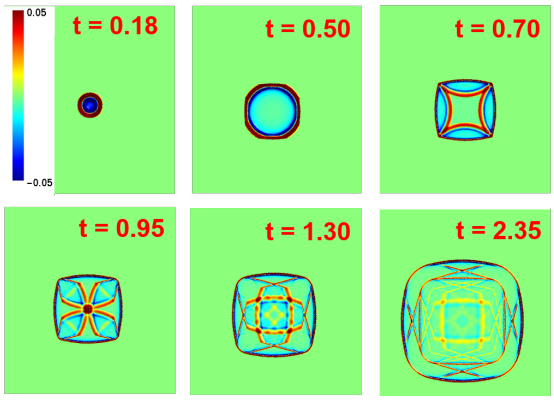

Figure 3: Time sequence; H_3 mapped to color.